The electronic, optical, and thermodynamical properties of tetragonal, monoclinic, and orthorhombic M_3N_4 (M = Si, Ge, Sn): A first-principles study*

Dong Chen(陈东)[1,†], Ke Cheng(程科)[2], and Bei-Ying Qi(齐蓓影)[1]

[1] College of Physics and Electronic Engineering, Xinyang Normal University, Xinyang 464000, China
[2] College of Optoelectronic Technology, Chengdu University of Information Technology, Chengdu 610025, China

(Received 25 December 2016; revised manuscript received 19 January 2017; published online 20 February 2017)

A detailed study of the M_3N_4 (M = Si, Ge, Sn) nitrides in their tetragonal, monoclinic and orthorhombic phases has been performed with the plane-wave pseudo-potential method combined with the quasi-harmonic approximation, including the phononic effects. We rationalize the main puzzle, i.e., the fundamental properties of these phases are unclear, by calculating the crystal structures, density of states, and optical properties. The direct band gaps of t-Ge_3N_4, m-Si_3N_4, and o-Ge_3N_4 benefit the opto–electrical properties. t-, m-, and o-Si_3N_4 can be used as refractive materials while m-M_3N_4 (M = Si, Ge, Sn) are optically transparent in the visible light region. Our results improve the understanding of the detailed electronic structures of all compounds, as well as the influences of electronic structure on their stabilities. Furthermore, we find that thermodynamic quantities are sensitive to structures and, therefore, depend on various temperature and pressure conditions.

Keywords: first-principles, density of states, optical properties, nitrides

PACS: 63.20.dk, 71.20.–b, 74.25.Gz, 81.05.Je **DOI:** 10.1088/1674-1056/26/4/046303

1. Introduction

With outstanding chemical and mechanical properties, group-IV nitrides M_3N_4 (M = Si, Ge, Sn, etc.) are considered as the most promising technological ceramics used in high-temperature fields.[1,2] The high fracture toughness, unique physical property and good thermal shock resistance make Si_3N_4 a desirable material for hostile environments.[3] The Si_3N_4 nitrides can also be used as wide-gap semiconductors, laser diodes and etch masks due to their high hardnesses and good thermal stabilities.[4,5] Under ambient conditions, there are two well-established polymorphs of Si_3N_4, namely the hexagonal α ($P31c$) and β ($P6_3/m$) phases, where the β configuration is the low-temperature phase and α-Si_3N_4 is often recognized as a metastable phase.[6] Several decades ago, the α- and β-Si_3N_4 were the only two phases known to exist.[7,8] Through the diamond anvil cell technique, the first work gave a temperature of 2000 K and a pressure of 15 GPa needed to synthesis the spinel γ phase (Fd-$3m$).[9] Several polymorphs of Si_3N_4 have been reported so far, including the still ambiguous phases {willemite-II-Si_3N_4 (I-$43d$),[10] δ-Si_3N_4($P3$),[7] post-spinel-Si_3N_4 ($BBMM$),[11] $P\bar{6}$ and $P\bar{6}$'-Si_3N_4($P3$),[7] etc}.

The group IV nitride usually displays desirable properties including enhanced wear resistance in Si_3N_4, unique catalytic activity in Ge_3N_4, and tunable band gap in Sn_3N_4.[12] Due, in particular, to its outstanding heat conductivity, electro–optical and dielectric properties, germanium nitride (Ge_3N_4) is a prospective compound for applications in photocatalysts, optical fibers, and engineering ceramics. It has been considered for applications as passivation layers, as possible negative electrodes, and as components of read-and-write memories.[13,14] Since carriers in Ge have higher mobilities compared with those in Si, the Ge-based field-effect-transistor has attracted a great deal of attention as a high-performance device. Sn_3N_4 is of special interest due to its electro–chromic and semiconducting properties. From an indentation technique, γ-Sn_3N_4 was found to be much softer and more plastic than its former congeners γ-Si_3N_4 and γ-Ge_3N_4.[15] The existence of α- and β-Ge_3N_4 has been identified in the synthesized nanobelts.[16] Progress has been rapid, and now the dense nitrides γ-M_3N_4 (M = Si, Ge, Sn) have already been synthesized and start to be commercially available.[17] It is worthy of note that Sn_3N_4 is far less studied than its silicon and germanium counterparts, and the investigation remains ongoing.

Nowadays, Xu *et al.*[7] and Kuwabara *et al.*[8] proposed calculations for the phonon dispersions, density of states, thermal properties and phase stabilities of α-, β-, and γ-Si_3N_4 through the VASP code. Gao *et al.*[18] and Luo *et al.*[19] have investigated the band structures, elastic moduli, thermodynamic properties and phase transitions of α-, β-, and γ-Ge_3N_4 using the plane-wave pseudo-potential method. The electronic and optoelectronic properties of α-, β-, and γ-M_3N_4 (M = Si, Ge, Sn) have been analysed by Caskey *et al.*[12] Detailed studies of the electronic, optical and thermodynamic properties of these nitrides have already been introduced in our previous works.[19,20] In 2015, Cui *et al.*[21] explored three

*Project supported by the National Natural Science Foundation of China (Grant Nos. 61475132 and 61501392).
†Corresponding author. E-mail: chchendong2010@163.com
© 2017 Chinese Physical Society and IOP Publishing Ltd

new polymorphs (tetragonal t-Si_3N_4, monoclinic m-Si_3N_4 and orthorhombic o-Si_3N_4) using the CALYPSO code.[22] Up to now, the fundamental properties of these compounds are still under development. For the purpose of structural consistency, we chose to describe tetragonal, monoclinic and orthorhombic Ge_3N_4 and Sn_3N_4, since α-, β-, and γ-Ge_3N_4/Sn_3N_4 (similar to silicon nitrides) had already been discovered. Consider the fact that the electronic structures between Ge/Sn and Si are quite similar, the t-, m-, and o-Ge_3N_4/Sn_3N_4 may also exist. The aim of this work is to predict the structural, electronic, optical and thermodynamic properties of t-, m-, and o-M_3N_4 (M = Si, Ge, Sn). We hope that our theoretical prediction will motivate future studies.

2. Model and methods

The optimized structures of Si_3N_4, Ge_3N_4, and Sn_3N_4 can be found in Refs. [23] and [24]. In this work, theoretical calculations were performed in the framework of density functional theory (DFT) using the plane-wave pseudopotential (PW-PP) method,[25] where the Perdew–Burke–Ernzerhof (PBE) functional[26] with generalized gradient approximation (GGA) was adopted to describe the exchange-correlation potentials.[27] The interactions between valence electrons and ionic cores are modeled by the Vanderbilt-type ultrasoft pseudo-potentials.[28] The electronic wave function is expanded in a plane wave basis set with a well converged cut-off energy of 500 eV for all cases. The Brillouin zones were sampled with the Monkhorst–Pack k-points[29] of 12×12×8, 8×18×12, and 11×7×10 for the tetragonal, monoclinic and orthorhombic phases, respectively. Pseudo-atomic valence states had been set as Si-$3s^2 3p^2$, Ge-$4s^2 4p^2$, Sn-$5s^2 5p^2$, and N-$2s^2 2p^3$. For the electronic structure calculations, the empty bands were chosen to be 53. The pristine lattice structures (including atomic positions) were relaxed through the Broyden–Fletcher–Goldfarb–Shanno (BFGS) scheme[30] with the following tolerances: energy difference per atom, maximum Hellmann–Feynman force, maximum ionic displacement, and maximum stress less than 1×10^{-6} eV, 0.01 eV/Å, 0.001 Å, and 0.02 GPa, respectively. The electronic, optical and thermodynamic properties are predicted based on the optimized structures.

In the full-electronic quasi-harmonic approximation (QHA) scheme,[31] the non-equilibrium Gibbs free energy $G^*(V;P,T)$ can be written as

$$G^*(V;P,T) = E(V)+PV+F_{\rm vib}(V;T) +F_{\rm el}(V;T)+F_{\rm res}(V;T), \quad (1)$$

where $E(V)$ is the total energy, P represents the external pressure, V is the cell volume, and $F_{\rm res}$ represents the reminder of the polynomial (magnetic, configurational, etc.).[31] $F_{\rm vib}$ and $F_{\rm el}$ are the contributions to the Helmholtz free energy from lattice vibrations and mobile electrons, respectively.

$$F_{\rm vib}(V;T) = \sum_{j=1}^{3nN}\left[\frac{\omega_j}{2}+k_{\rm B}T\ln(1-{\rm e}^{-\omega_j/k_{\rm B}T})\right],$$
$$F_{\rm el}(V;T) = \frac{1}{4}\pi^2T^2k_{\rm B}^2\frac{n_{\rm el}}{E_{\rm F}}, \quad (2)$$

where $E_{\rm F}$ is the Fermi level, $k_{\rm B}$ Boltzmann's constant, $n_{\rm el}$ the number of valence electrons, T the temperature, ω_j the vibrational frequency, n the number of atoms, and N the number of cells. Thermal properties such as heat capacity C_v, C_p, isothermal bulk modulus B, internal energy U, thermal expansion coefficient α, Grüneisen parameter γ, and entropy S can be derived from Eq. (1)

$$C_v = 3nk_{\rm B}\left[4D(\theta/T)-\frac{3\theta/T}{{\rm e}^{\theta/T}-1}\right],$$
$$C_p = C_v(1+\gamma\alpha T),\quad B = V\left[\frac{\partial^2 G*(V;P,T)}{\partial V^2}\right]_T, \quad (3)$$
$$U = F+TS = E+\sum_j\frac{\omega_j}{2}+\sum_j\frac{\omega_j}{{\rm e}^{-\omega_j/k_{\rm B}T}-1}, \quad (4)$$
$$\alpha = \frac{\gamma C_v}{VB_T},\quad \gamma = -\frac{V}{TC_v}\left(\frac{\partial(-TS)}{\partial V}\right), \quad (5)$$
$$S = \sum_j\left[-k_{\rm B}\ln(1-{\rm e}^{-\omega_j/k_{\rm B}T})+\frac{\omega_j}{T}\frac{1}{{\rm e}^{\omega_j/k_{\rm B}T}-1}\right], \quad (6)$$

where V is the volume, P the pressure, θ the Debye temperature, and $D(\theta/T)$ the Debye integral, respectively. The detailed expressions of QHA can be found in Refs. [31] and [32]. The mobile electrons can be ignored in semiconductors.

3. Results and discussions

3.1. Crystal structures

As a first step, the M_3N_4 (M = Si, Ge, Sn) crystals have been optimized. The results are listed in Table 1. It is shown that the calculated lattice constants a, b, c and elastic moduli B, G, E of Si_3N_4 are consistent with the literature,[21] while the maximum relative errors are only 0.9% and 8.5% for the lattice constants and elastic moduli, respectively (within the general accuracy of GGA, i.e., 1%∼3% for lattice constants and 1%∼10% for elastic moduli). The bulk moduli B are greater than the shear moduli G, which reflects that the principal parameter limiting the stabilities of t-, m-, and o-M_3N_4 (M = Si, Ge, Sn) is the shear modulus.[33] Since B is a measure of rigidity, we conclude that the rigidity of the orthorhombic phase is the highest among these polymorphs. Young's modulus E follows the sequences Si_3N_4 >Ge_3N_4 >Sn_3N_4 and orthorhombic > tetragonal > monoclinic. In Table 1, it is found that all nitrides show semiconducting characteristics. The direct band gap enables the direct transitions of electrons, which is beneficial to the opto–electrical properties of t-Ge_3N_4, m-Si_3N_4,

and o-Ge_3N_4. The remaining compounds show indirect band gaps. Si_3N_4 are wide band-gap (> 3 eV) semiconductors while Ge_3N_4 and Sn_3N_4 belong to narrow band-gap (< 3 eV) semiconductors. Although Cui *et al.*[21] found that m-Si_3N_4 belongs to direct band gap semiconductor (Γ_V–Γ_C); our result shows that m-Si_3N_4 has an A_V–A_C direct band gap.

It is worth noting that DFT + GGA usually underestimate the band gaps of nitrides, hence the real band gaps of M_3N_4 (M = Si, Ge, Sn) would be wider than the predicted values. In Table 1, the B_a is the bulk modulus obtained by the quasi-harmonic approximation (i.e., QHA bulk modulus), while B represents the first-principles PW–PP bulk modulus. For most cases, the B_a and B agree well with each other. Frankly speaking, the reason for the discrepancy between B_a and B (for t-Ge_3N_4) is still unclear. This needs to be testified by future expertiments. On one hand, we have thoroughly studied the elastic constants C_{ij} of t-, m-, and o-Si_3N_4/Ge_3N_4 in our previous works.[23,24] On the other hand, our calculated lattice constants, elastic constants, bulk moduli and thermal properties of α-Si_3N_4, β-Si_3N_4, γ-Si_3N_4, β-Ge_3N_4, and γ-Ge_3N_4 are in agreement with the experimental data.[19,34,35] These facts partially demonstrate that our results given in this work are reliable but need to be verified by future experiments.

Table 1. Calculated equilibrium structural parameters: lattice constants a, b, c, bulk modulus B, shear modulus G, Young's modulus E, and band gap E_g for t-, m-, and o-M_3N_4 (M = Si, Ge, Sn).

	a/nm	b/nm	c/nm	B/GPa	G/GPa	E/GPa	B_a/GPa	E_g/eV
t-Ge_3N_4	0.4410	0.4410	0.8835	146.8	86.8	217.7	194.5	1.76 (Γ–Γ)
m-Ge_3N_4	1.0215	0.3103	0.7928	124.1	72.8	182.8	126.9	1.85 (A–Γ)
o-Ge_3N_4	0.5256	1.0074	0.5317	203.4	122.0	305.1	198.4	1.35 (Γ–Γ)
t-Sn_3N_4	0.4930	0.4930	0.9961	84.9	38.6	100.5	85.8	0.22 (M–Γ)
m-Sn_3N_4	1.1473	0.3487	0.8891	74.4	33.5	87.3	83.3	0.13 (E–Γ)
o-Sn_3N_4	0.5845	1.1164	0.5904	150.6	80.4	204.7	140.7	0.16 (Γ–Y)
t-Si_3N_4	0.4166	0.4166	0.8249	194.4	126.1	311.0	195.2	3.04 (M–Γ)
m-Si_3N_4	0.9603	0.2932	0.7419	165.4	104.3	258.5	171.1	3.77 (A–A)
o-Si_3N_4	0.4937	0.9426	0.4948	261.5	178.6	436.4	265.7	3.21 (Γ–Y)
t-Si_3N_4[21]	0.4131	0.4131	0.8168	193.8	134.9	328.4	–	3.15 (M–Γ)
m-Si_3N_4[21]	0.9512	0.2904	0.7353	164.9	113.2	276.3	–	3.90 (Γ–Γ)
o-Si_3N_4[21]	0.4901	0.9356	0.4910	258.1	185.7	449.3	–	3.36 (Γ–Y)

3.2. Electronic properties

The total density of states (TDOS) and partial-wave density of states (PDOS) projected onto different atoms, obtained, respectively, with single M_3N_4 (M = Si, Ge, Sn) unit (7 atoms), are plotted in Fig. 1. At first glance, it appears that the TDOSs of t-M_3N_4 (M = Si, Ge, Sn) drawn in Fig. 1(a) differ very little. It is clear that the DOS at Fermi level E_F is dominated by the contribution of N-2p orbital in combination with the weak contributions of M-s, p states. The valence band (VB) can be separated into two parts: i.e. the lower region and the upper region. The lower VB region (from about -18 eV to -12 eV) consists mainly of N-2s band hybridized with small contributions from M-s and M-p orbitals. The upper VB region from -9 eV to 0 eV is dominated by the M-s band, but hybridization occurs between the N-2p and M-p states. There are five well-resolved peaks that appear in the upper VB regions of t-M_3N_4 (M = Si, Ge, Sn). The conduction band (CB) DOS is also rich in structures while the Si and Sn elements have comparable contributions. The Ge contribution to CB is significant. In Figs. 1(b), 1(c), and 1(d), PDOSs of t-Si_3N_4, t-Ge_3N_4, and t-Sn_3N_4 show the same variation with energy. In the PDOS of t-Ge_3N_4, the lower VB region is dominated by s electrons of N and Ge, and the upper VB region is mainly composed of N-2p states (unlike t-Si_3N_4/Sn_3N_4). Follow the sequence Si_3N_4 $\rightarrow$$Ge_3N_4$ $\rightarrow$$Sn_3N_4$, the peaks of lower VB-DOSs increase, reflecting the enhanced M–N hybridization. The VB-DOSs of Si_3N_4 and Ge_3N_4 are broader than that of Sn_3N_4 by approximately 2.4 eV and 2.2 eV, respectively. This is caused by the Sn atom because its s-electrons are located near the bottom of the VB, which indicates that Sn_3N_4 are the most stable compounds among the three nitrides.

The DOSs of m- and o-M_3N_4 (M = Si, Ge, Sn) are plotted in Figs. 2 and 3, respectively. Like Fig. 1, TDOSs drawn in Figs. 2(a) and 3(a) look similar on the gross scale. The reasons may be (i) the same crystal structure; (ii) Ge and Sn are iso-electronic elements. A subtle difference in the CB peaks can be noticed, which is due to the different atomic contributions in Si_3N_4, Ge_3N_4, and Sn_3N_4. For example, PDOSs of Ge/Sn at different coordinations are somehow different in the peak intensities indicating the difference of local environment. The sharp VB edge of M_3N_4 (M = Si, Ge, Sn) implies that a lot of electrons may be distributed there. The valence band maxima are dominated by the p-orbitals of nitrogen atoms.[36] The monoclinic phases plotted in Figs. 2(b), 2(c), and 2(d) show some differences, which are related to the atomic coordination and lattice constant (hence the bond length). As shown in Figs. 3(b), 3(c), and 3(d), the DOSs of orthorhombic phases are much higher than the DOSs of tetragonal and mon-

oclinic phases. Comparing with Ge_3N_4 and Si_3N_4, Sn_3N_4 has a steeper VB edge, a smaller band gap, and a less sharp CB edge. The interactions among different orbitals demonstrate the strong covalent Si/Ge/Sn–N bonding. The VB band width obeys the rule Si_3N_4 >Ge_3N_4 >Sn_3N_4. The bonding interactions between M and N atoms play an important role in the stabilities of M_3N_4 (M = Si, Ge, Sn).

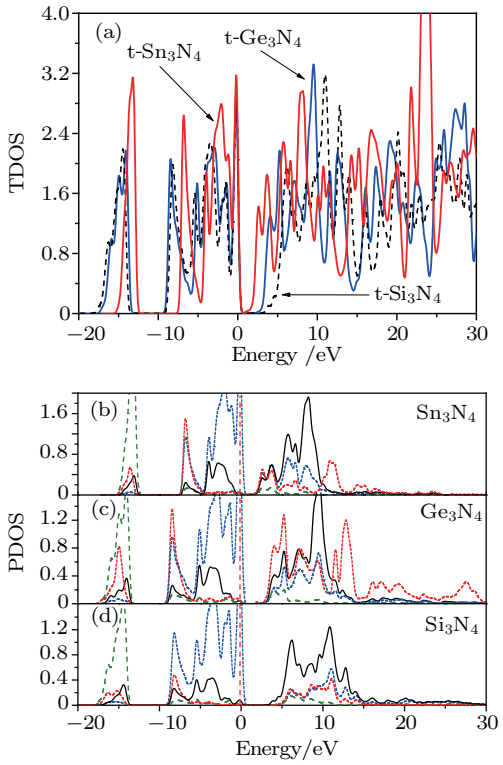


Fig. 1. (color online) Total density of states for t-M_3N_4 (M = Si, Ge, Sn) (a), partial density of states for t-Sn_3N_4 (b), t-Ge_3N_4 (c), and t-Si_3N_4 (d). In panels (b), (c), and (d), the red/dashed, black/solid, green/dashed, and blue/dashed curves represent the M-s, M-p, N-s, and N-p states, respectively.

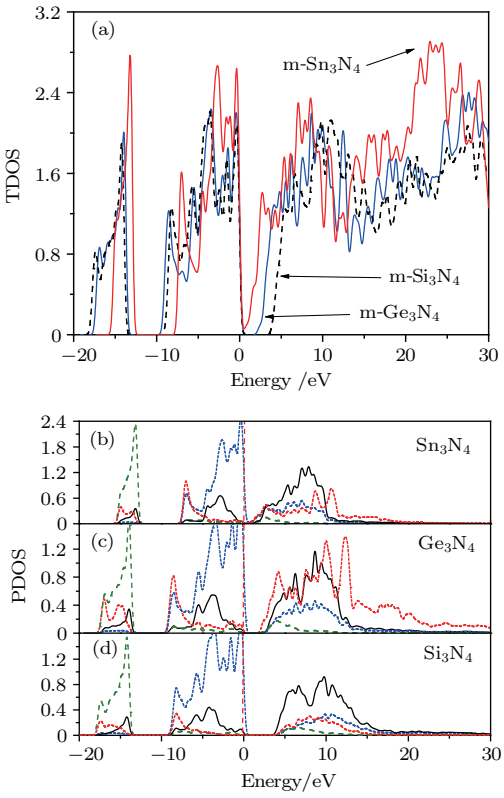


Fig. 2. (color online) The same as Fig. 1, but for m-M_3N_4 (M = Si, Ge, Sn).

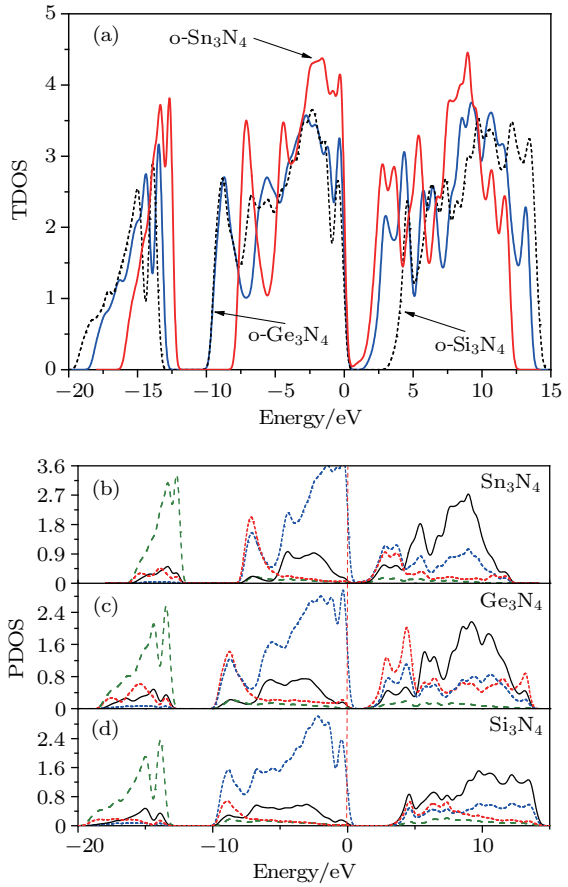


Fig. 3. (color online) The same as Fig. 1, but for o-M_3N_4 (M = Si, Ge, Sn).

3.3. Thermodynamic properties

The isobaric heat capacity C_P is an important parameter indicating the loss ability and heat retention. Although the constant-volume heat capacity C_v gives direct information of anharmonic effects, it is C_P that is experimentally measured, and it contains both the anharmonic effect and quasi-harmonic contribution leading to its departure from the Dulong–Petit's limit (C_v ∝3R for monoatomic materials).[37] In Fig. 4, one can see that the heat capacities of t-, m-, and o-M_3N_4 (M = Si, Ge, Sn) are quite similar in appearance. From 0 K to 300 K, the heat capacities follow the Debye law ($C_P \propto T^3$) and vanish when the temperature tends to zero. Then, C_P gradually reaches an almost linear region (300 K∼800 K) and the increasing trend becomes gentler. When T > 800 K, C_P increases monotonically with the rising of temperature (due to anharmonic effects), which is common to all solids at high temperatures. As shown in Fig. 4(a), the temperature effect on the heat capacity of t- and m-Si_3N_4 is more significant than that on o-Si_3N_4. In Fig. 4(b), the three curves show that C_P dependences on temperature are quite similar. For Sn_3N_4, the tetragonal and monoclinic phases have larger heat capacities than the orthorhombic phase. The knee points (at 200 K)

shown in Fig. 4(c) also demonstrate that C_P of Sn_3N_4 increases more rapidly than the curves of Si_3N_4 and Ge_3N_4.

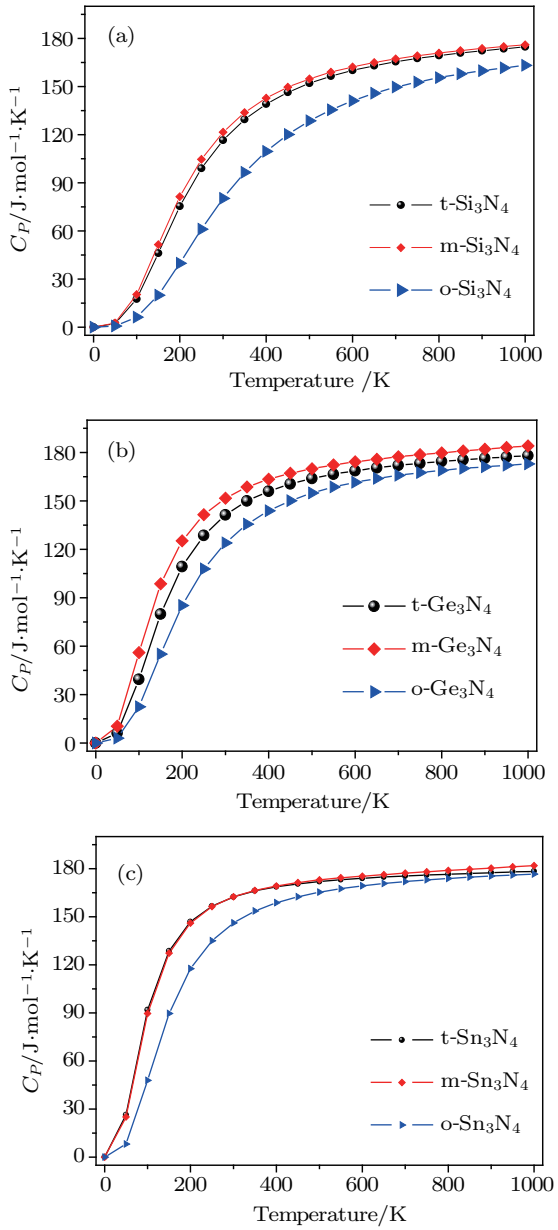


Fig. 4. (color online) Temperature-dependent isobaric heat capacity C_P of the tetragonal, monoclinic, and orthorhombic phases for (a) Si_3N_4; (b) Ge_3N_4, and (c) Sn_3N_4.

Microscopic entropy can be defined as a measure of the disorder of a compound. As expected, this parameter is highly dependent on the temperature T. Figure 5 shows the zero-pressure entropy S versus temperature for Si_3N_4, Ge_3N_4, and Sn_3N_4. As a non-purely-anharmonic quantity, one could not expect the linear relationship between S and T. It is clearly seen that S nearly keeps unchanged when $T < 50$ K. In the temperature range of 50 K∼600 K, the entropies are variable by power exponent with the temperature increasing. At higher temperatures, S increases almost linearly with enhanced temperature. As shown in Fig. 5(a), the curves are essentially indistinguishable below 100 K. The highest entropy is m-Si_3N_4, followed by t-Si_3N_4 and o-Si_3N_4. In Fig. 5(b), the discrepancy of S increases with applied temperature. As plotted in Fig. 5(c), the entropies of t-Sn_3N_4 and m-Sn_3N_4 are nearly the same in the whole temperature range of 0 K∼1000 K. It is worthy of note that the entropies of Si_3N_4 are much lower than those of Ge_3N_4 and Sn_3N_4. The results show that Sn_3N_4 has the lowest entropy. The effect of temperature on S is more significant at high temperature than that at low temperature. It is due mainly to the fact that as the temperature increases the lattice atoms vibrate more vigorously, inducing an increase in entropy.

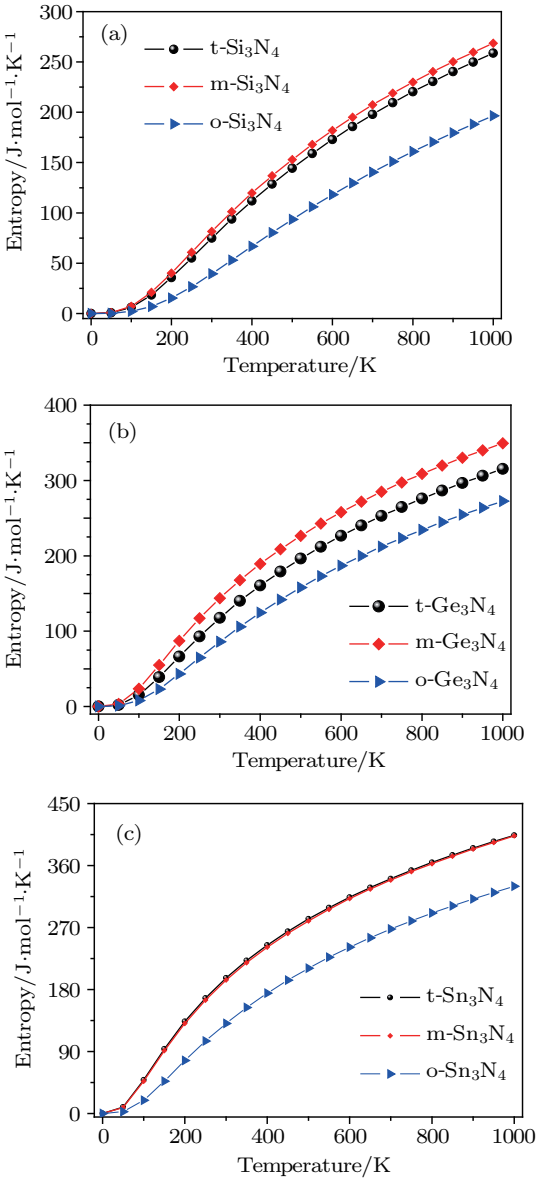


Fig. 5. (color online) Temperature-dependent entropy S of the tetragonal, monoclinic, and orthorhombic phases for (a) Si_3N_4; (b) Ge_3N_4, and (c) Sn_3N_4.

The normalized vibrational internal energy U/U_0 (U_0 is the zero-temperature vibrational internal energy) is plotted in Fig. 6(a). One can see that U/U_0 increases with temperature for all compounds (especially at $T > 100$ K), and gradually tends to the linear increases at higher temperatures, but the slopes are different. The nine curves coincide at 0 K and diverge more and more when the temperature increases. These

U/U_0 curves are almost unchanged in the temperature range of 0 K$\sim$ 100 K. Our results show a rather dramatic increase in U/U_0 (t-Sn_3N_4) with T until the temperature tends to 1000 K. At a fixed temperature, m-Sn_3N_4 has a slightly lower U/U_0 than t-Sn_3N_4. Finally, the increasing trend of U/U_0 while going from Sn_3N_4 (fastest), to Ge_3N_4 (moderate) and to Si_3N_4 (slowest). The Grüneisen parameter γ, which describes the alteration in the lattice vibrations, can predict the anharmonic properties of crystals, such as the temperature-dependent Debye frequency and cell volume. Consequently, the Grüneisen parameters of t-, m-, and o-M_3N_4 (M = Si, Ge, Sn) are drawn in Fig. 6(b).

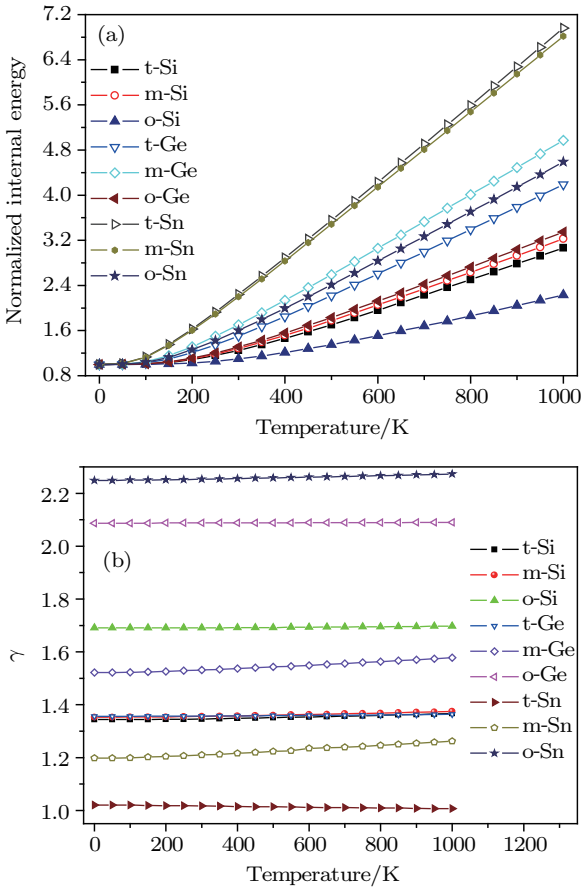


Fig. 6. (color online) Temperature dependences of the fundamental properties of t-, m-, and o-M_3N_4 (M = Si, Ge, Sn): (a) normalized internal energy U/U_0; (b) Grüneisen parameter γ.

As shown in Fig. 6(b), the Grüneisen parameter γ increases slightly with the temperature increasing, indicating that the anharmonicities of these compounds are not closely related to the temperature. The temperature effect on γ is not as significant as that on C_P and S. In the temperature range of 0 K$\sim$1000 K, γ of t-Sn_3N_4 decreases by 1.27%, while γ of t-Si_3N_4, m-Si_3N_4, o-Si_3N_4, t-Ge_3N_4, m-Ge_3N_4, o-Ge_3N_4, m-Sn_3N_4, and o-Sn_3N_4 increase by 1.71%, 1.63%, 0.35%, 0.59%, 3.68%, 0.14%, 5.34%, and 1.07%, respectively. The ratio of orthorhombic phase is highest followed by the monoclinic phase, the tetragonal phase possesses the least. The effect of temperature is more pronounced for m-Sn_3N_4. The predicted heat capacity C_P ($S/U/\gamma$) for t-Si_3N_4, m-Si_3N_4, o-Si_3N_4, t-Ge_3N_4, m-Ge_3N_4, o-Ge_3N_4, t-Sn_3N_4, m-Sn_3N_4, and o-Sn_3N_4 are

116.5 (74.9/73.8/1.35), 121.5 (81.5/71.7/1.36),
80.3 (39.4/92.9/1.69), 141.3 (117.6/63.9/1.36),
151.7 (143.8/60.5/1.53), 124.0 (85.9/70.5/2.09),
162.3 (196.7/56.6/1.02), 162.4 (193.8/56.7/1.21),

and 146.1 J·mol^{-1}·K^{-1} (130.8 J·mol^{-1}·K^{-1}/62.0 kJ·mol^{-1}/2.25), respectively. Note that we could not find any other results for our comparison. Hence our calculation can serve as a prediction for future study of the thermal properties of M_3N_4 (M = Si, Ge, Sn).

3.4. Optical properties

Optical properties of solids are defined by the complex dielectric function $\varepsilon(\omega) = \varepsilon_1(\omega) + i\varepsilon_2(\omega)$, where $\varepsilon_1(\omega)$ is the real part of the dielectric function and $\varepsilon_2(\omega)$ is the imaginary part of the dielectric function. The real part is determined from the imaginary part using the Kramers–Krönig relations.[38] $\varepsilon_1(\omega) < 0$ means that light cannot spread the material in the corresponding energy region. It can be seen that the spectrum shapes of the real part of Ge_3N_4/Sn_3N_4, which are shown in Figs. 7(a), 7(b), and 7(c), are similar. During the photon energy increased process, $\varepsilon_1(\omega)$ reaches the highest values of 7.26 (at 7.05 eV), 6.48 (at 6.07 eV), 8.82 (at 6.22 eV), 8.35 (at 5.47 eV), 7.27 (at 4.24 eV), 10.28 (at 2.95 eV), 8.81 (at 2.65 eV), 9.54 (at 0 eV), and 10.85 (at 2.06 eV), and then decreases to the valleys of -2.23 (at 14.82 eV), -1.48 (at 14.71 eV), -3.27 (at 13.86 eV), -2.04 (at 13.57 eV), -1.30 (at 13.36 eV), -2.77 (at 12.04 eV), -1.54 (at 11.17 eV), -1.24 (at 10.79 eV), and -2.24 (at 10.72 eV) for t-Si_3N_4, t-Ge_3N_4, t-Sn_3N_4, m-Si_3N_4, m-Ge_3N_4, m-Sn_3N_4, o-Si_3N_4, o-Ge_3N_4, and o-Sn_3N_4, respectively. The static dielectric constant $\varepsilon_1(0)$ is found to be 4.47, 4.24, 5.71, 5.59, 5.30, 8.13, 7.69, 9.54, and 10.57 for t-Si_3N_4, t-Ge_3N_4, t-Sn_3N_4, m-Si_3N_4, m-Ge_3N_4, m-Sn_3N_4, o-Si_3N_4, o-Ge_3N_4, and o-Sn_3N_4, respectively. $\varepsilon_1(0)$ of t-, m-, and o-Si_3N_4 are much smaller than those of elemental semiconductors Si and Ge, but are larger than α-, β- and γ-Si_3N_4.[39] m- and t-Sn_3N_4 have the highest dielectric constants than any other compound; hence they can be used as candidates for dense refractive materials.

The imaginary dielectric function $\varepsilon_2(\omega)$ represents the optical absorption of solids. Large difference of the dielectric functions $\varepsilon_2(\omega)$ can be seen in Fig. 7, where the peaks are obviously shifted in different compounds. It is clearly observed in Figs. 7(d) and 7(e) that there are two peaks in the imaginary part of t- and m-Si_3N_4, the main peaks of t-Sn_3N_4 (m-Si_3N_4) are located at 4.69 (10.31) and 8.44 (12.56) eV. Each spectrum shown in Fig. 7(f) has a prominent absorption peak. The three main peaks at 4.99, 6.21, and 9.51 eV for

o-Si_3N_4, o-Ge_3N_4, and o-Sn_3N_4 have also been revealed, respectively. The amplitude of the main peak in the orthorhombic phase is significantly higher than the peaks in the other two phases. The maxima of $\varepsilon_1(\omega)$ and $\varepsilon_2(\omega)$ for the nine compounds have shifted to the low energy region following the sequence $Si_3N_4 \rightarrow Ge_3N_4 \rightarrow Sn_3N_4$. In Fig. 7(d), the rising curves show that the first optical point arises at 3.6 (2.2/0) eV for t-Si_3N_4 (t-Ge_3N_4/t-Sn_3N_4). This is due to the fact that the number of points contributing toward $\varepsilon_2(\omega)$ is enhanced abruptly. It is also noted that the spectral shape of m-Si_3N_4 is little dissimilar from the other compounds, demonstrating somehow the different bonding nature of this system.

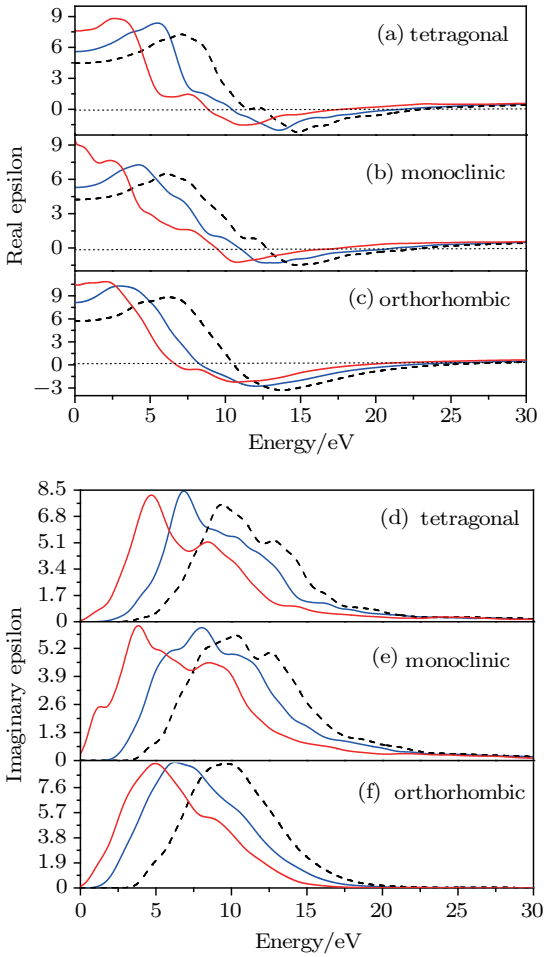


Fig. 7. (color online) Real part of dielectric function $\varepsilon_1(\omega)$ for different M_3N_4 (M = Si, Ge, Sn) polymorphs: (a) tetragonal; (b) monoclinic; (c) orthorhombic. Imaginary part of dielectric function $\varepsilon_2(\omega)$ for different polymorphs: (d) tetragonal; (e) monoclinic; (f) orthorhombic. The black/dashed, blue/solid, and red/solid curves represent the Si_3N_4, Ge_3N_4, and Sn_3N_4 compounds, respectively.

The reflectivity $R(\omega)$ of different nitrides is plotted in Figs. 8(a), 8(b), and 8(c). As deducible from the dielectric function, up to the sharp plasma edge, all main peaks cause from inter-band transitions and for higher energies, the reflectivity vanishes. The maximum $R(\omega)$ of the above-mentioned nitrides appears in the energy range between 10 eV and 25 eV. As shown in Fig. 8(a), the $R(\omega)$ begins to increase from a relatively small value (12.71% for t-Si_3N_4, 16.52% for t-Ge_3N_4, and 22.10% for t-Sn_3N_4) to attain a maximum value (50.22% for photon energy at 17.11eV for t-Si_3N_4, 48.90% for photon energy at 14.21 eV for t-Ge_3N_4, and 43.62% for photon energy at 12.45 eV for t-Sn_3N_4). Then, the $R(\omega)$ decreases with the increasing photon energy. In Fig. 8(b), the curves do not exceed 40% through the whole energy range of 0 eV∼40 eV, indicating that the monoclinic M_3N_4 (M = Si, Ge, Sn) are transparent materials. These nitrides may find applications as transparent coatings in the visible light region (1.6 eV∼3.0 eV). For the orthorhombic phase shown in Fig. 8(c), the $R(\omega)$ is higher than 50% in the energy range of 12 eV∼20/25 eV, indicating that photons in this energy region cannot travel through the solid. The sharp reflectivity plasma edges are located at 19.5, 23, and 25 eV for o-Si_3N_4, o-Ge_3N_4, and o-Sn_3N_4, respectively.

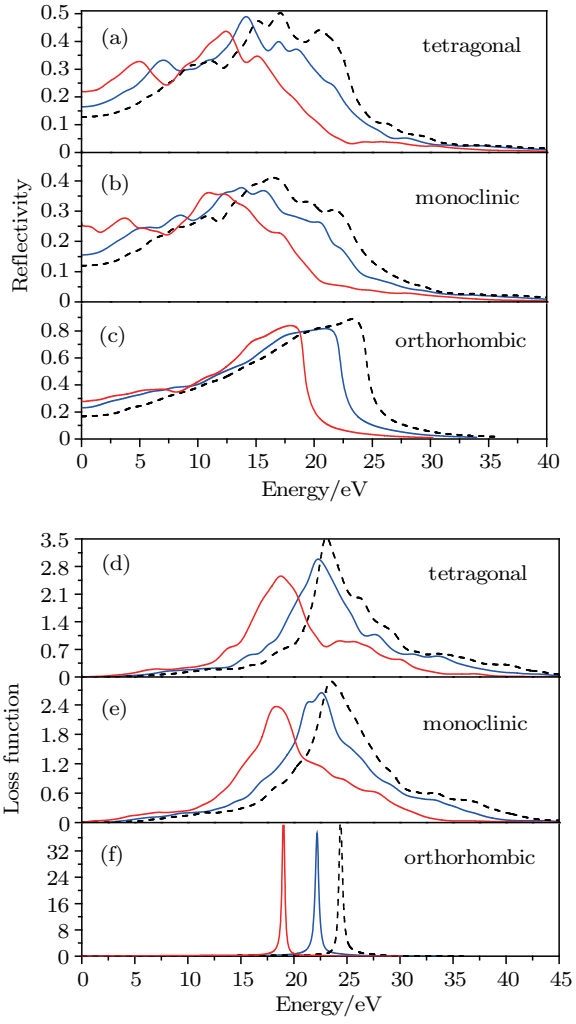


Fig. 8. (color online) Reflectivity curves of different M_3N_4 (M = Si, Ge, Sn) polymorphs: (a) tetragonal; (b) monoclinic; (c) orthorhombic. Loss function of different polymorphs: (d) tetragonal; (e) monoclinic; (f) orthorhombic. The black/dashed, blue/solid, and red/solid curves represent the Si_3N_4, Ge_3N_4, and Sn_3N_4 compounds, respectively.

The photon energy dependences of energy loss function $L(\omega)$ are plotted in Figs. 8(d), 8(e), and 8(f). $L(\omega)$ describes the energy-loss of a fast electron traversing in the material.[40] The peak of $L(\omega)$ describes the characteristic of plasma oscillation, the frequency of collective oscillation of the valence electrons. The dominant peaks in the loss function, which are

due mainly to a longitudinal oscillation of the valence electrons as whole against the cores, have been found to locate at approximately 19.0, 22.2, and 24.5 eV for Si_3N_4, Ge_3N_4, and Sn_3N_4, respectively. These peaks correspond to the rapid reduction of $R(\omega)$. In Figs. 8(d) and 8(e), the main peaks are broad, which are due mainly to the contributions of N-2p to M-p transitions. Furthermore, some small peaks are observed in t-Ge_3N_4, t-Sn_3N_4, and m-Ge_3N_4 which indicate weak resonances. It can be seen in Fig. 8(f) that the orthorhombic phases have enhanced amplitudes in $L(\omega)$ compared with the tetragonal and monoclinic phases. Unfortunately, no optical data are available in the literature for our comparison.

4. Conclusions

We have investigated the structural, electronic, optical and thermodynamic properties of M_3N_4 (M = Si, Ge, Sn) in their tetragonal, monoclinic and orthorhombic phase based on first-principles calculations combined with a quasi-harmonic approach (QHA). The calculated lattice constants, band gaps and elastic moduli of t-, m-, and o-Si_3N_4 are in agreement with the experimental data. t-Ge_3N_4, m-Si_3N_4, and o-Ge_3N_4 have direct band gaps. The strong covalent bonds between N-2p and M-s, p orbitals of the orthorhombic phases are attributed to the optimal arrangement of cations, which play an important role in the stabilities of M_3N_4 (M = Si, Ge, Sn). The major trend in thermodynamic quantities shows that the nitrides become more compressible when the temperature is enhanced. The higher temperatures usually lead to higher entropies, larger internal energies and fixed Grüneisen parameters. The dielectric function of m-Si_3N_4 is little dissimilar from the other systems, reflecting its different bonding nature. The reflectivity shows that m-M_3N_4 (M = Si, Ge, Sn) are transparent materials. It is envisioned that proper mixing of (Si, Ge, Sn)$_3N_4$ in the tetragonal, monoclinic and orthorhombic phases may lead to compounds with superior optical properties. The calculation scheme presented in this work is a promising alternative for the determination of the physical properties of nitrides that are difficult or costly to obtain from experiments.

Acknowledgements

We thank Prof. Alberto Qtero-de-la-Roza and his colleagues for the Gibbs2 software. We also acknowledge Prof. M A Blanco and his co-workers for their Gibbs code.

References

[1] Jing J T, Feng P F, Wei S L, Zhao H and Liu Y F 2016 *Appl. Surf. Sci.* **387** 812
[2] Hou G L, Cheng B L, Ding F, Yao M S, Hu P and Yuan F L 2015 *ACS Appl. Mater. Interfaces* **7** 2873
[3] Lin Z X, Lin Z W, Zhang Y, Song C, Guo Y Q, Wang X, Huang X T and Huang R 2014 *Acta Phys. Sin.* **63** 037801 (in Chinese)
[4] Kim S J, Jung S H, Kim M H, Cho S J and Park B G 2015 *Appl. Phys. Lett.* **106** 212106
[5] Kalia R K, Nakano A, Tsuruta K and Vashishta P 1997 *Phys. Rev. Lett.* **78** 689
[6] Wang L G, Sun J X, Yang W and Tian R G 2008 *Acta Phys. Pol. A* **114** 807
[7] Xu B, Dong J J, McMillan P F, Shebanova O and Slamat A 2011 *Phys. Rev. B* **84** 014113
[8] Kuwabara A, Matsunaga K and Tanaka I 2008 *Phys. Rev. B* **78** 064104
[9] Zerr A, Miehe G, Serghiou G, Schwarz M, Kroke E, Riedel R, Fueß H, Kroll P and Boehler R 1999 *Nature* **400** 340
[10] Kroll P 2003 *J. Solid State Chem.* **176** 530
[11] Tatsumi K, Tanaka I, Adachi H, Oba F and Sekine T 2002 *J. Am. Ceram. Soc.* **85** 7
[12] Caskey C M, Seabold J A, Stevanović V, Ma M, Smith W A, Ginley D S, Neale N R, Richards R M, Lany S and Zakutayev A 2015 *J. Mater. Chem. C* **3** 1389
[13] Boyko T D, Hunt A, Zerr A and Moewes A 2013 *Phys. Rev. Lett.* **111** 097402
[14] Ding Y C, Chen M and Wu W J 2015 *J. Theor. Comput. Chem.* **14** 1550024
[15] Pradhan G K, Kumar A, Deb S K, Waghmare U V and Narayana C 2010 *Phys. Rev. B* **82** 144112
[16] Gao Y H, Bando Y and Sato T 2001 *Appl. Phys. Lett.* **79** 4565
[17] Zhang C, Sun J X, Tian R G and Zou S Y 2007 *Acta Phys. Sin.* **56** 5969 (in Chinese)
[18] Gao S P, Cai G H and Xu Y 2013 *Comput. Mater. Sci.* **67** 292
[19] Luo Y S, Cang Y P and Chen D 2014 *Comput. Condens. Matter* **1** 1
[20] Yu B H and Chen D 2013 *J. Alloys Compd.* **581** 747
[21] Cui L, Hu M, Wang Q Q, Xu B, Yu D L, Liu Z Y and He J L 2015 *J. Solid State Chem.* **228** 20
[22] Wang Y C, Lv J, Zhu L and Ma Y W 2010 *Phys. Rev. B* **82** 094116
[23] Cang Y P, Lian S B, Yang H M and Chen D 2016 *Chin. Phys. Lett.* **33** 066301
[24] Cang Y P, Chen D, Yang F and Yang H M 2016 *Chem. J. Chin. Univ.* **37** 674
[25] Kohn W and Sham L J 1965 *Phys. Rev.* **140** A1133
[26] Perdew J P, Burke K and Ernzerhof M 1996 *Phys. Rev. Lett.* **77** 3865
[27] Perdew J P, Chevary J A, Vosko S H, Jackson K A, Pederson M R, Singh D J and Fiolhais C 1992 *Phys. Rev. B* **46** 6671
[28] Vanderbilt D 1990 *Phys. Rev. B* **41** 7892
[29] Monkhorst H J and Pack J D 1976 *Phys. Rev. B* **13** 5188
[30] Pfrommer B G, Côté M, Louie S G and Cohen M L 1997 *J. Comput. Phys.* **131** 233
[31] Otero-de-la-Roza A, Abbasi-Pérez D and Luaña V 2011 *Comput. Phys. Commun.* **182** 2232
[32] Blanco M A, Francisco E and Luaña V 2004 *Comput. Phys. Commun.* **158** 57
[33] Peng S M 2015 *J. Nucl. Mater.* **464** 230
[34] Chen D and Yu B H 2013 *Chin. Phys. B* **22** 023104
[35] Yu B H and Chen D 2012 *Chin. Phys. B* **21** 060508
[36] Sevik C and Bulutay C 2007 *J. Mater. Sci.* **42** 6555
[37] Terki R, Bertrand G and Aourag H 2005 *Microelectron. Eng.* **81** 514
[38] Wooten F 1972 *Optical Properties of Solides* (New York: Academic Press)
[39] Xu Y N and Ching W Y 1995 *Phys. Rev. B* **51** 17379
[40] Hu C H, Yin X H, Wang D H, Zhong Y, Zhou H Y and Rao G H 2016 *Chin. Phys. B* **25** 067801